The Journal of Chemical Physics

On the use of DFT+*U* to describe the electronic structure of TiO_2 nanoparticles: $(TiO_2)_{35}$ as a case study

Cite as: J. Chem. Phys. **152**, 244107 (2020); https://doi.org/10.1063/5.0012271
Submitted: 29 April 2020 . Accepted: 04 June 2020 . Published Online: 22 June 2020

Ángel Morales-García, Stephen Rhatigan, Michael Nolan, and Francesc Illas

The Journal of Chemical Physics ARTICLE scitation.org/journal/jcp

On the use of DFT+*U* to describe the electronic structure of TiO_2 nanoparticles: $(TiO_2)_{35}$ as a case study

Cite as: J. Chem. Phys. 152, 244107 (2020); doi: 10.1063/5.0012271
Submitted: 29 April 2020 • Accepted: 4 June 2020 •
Published Online: 22 June 2020

Ángel Morales-García,[1] Stephen Rhatigan,[2] Michael Nolan,[2,a)] and Francesc Illas[1,b)]

AFFILIATIONS

[1] Departament de Ciència de Materials i Química Física & Institut de Química Teòrica i Computacional (IQTCUB), Universitat de Barcelona, c/Martí i Franquès 1-11, 08028 Barcelona, Spain
[2] Tyndall National Institute, University College Cork, Lee Maltings, Cork T12 R5CP, Ireland

[a)] **E-mail:** michael.nolan@tyndall.ie
[b)] **Authors to whom correspondence should be addressed:** francesc.illas@ub.edu

ABSTRACT

One of the main drawbacks in the density functional theory (DFT) formalism is the underestimation of the energy gaps in semiconducting materials. The combination of DFT with an explicit treatment of the electronic correlation with a Hubbard-like model, known as the DFT+*U* method, has been extensively applied to open up the energy gap in materials. Here, we introduce a systematic study where the selection of the *U* parameter is analyzed considering two different basis sets: plane-waves and numerical atomic orbitals (NAOs), together with different implementations for including *U*, to investigate the structural and electronic properties of a well-defined bipyramidal $(TiO_2)_{35}$ nanoparticle. This study reveals, as expected, that a certain *U* value can reproduce the experimental value for the energy gap. However, there is a high dependence on the choice of basis set and on the *U* parameter employed. The present study shows that the linear combination of the NAO basis functions, as implemented in Fritz Haber Institute *ab initio* molecular simulation (FHI-aims), requires, requires a lower *U* value than the simplified rotationally invariant approach, as implemented in the Vienna *ab initio* simulation package (VASP). Therefore, the transfer of *U* values between codes is unfeasible and not recommended, demanding initial benchmark studies for the property of interest as a reference to determine the appropriate value of *U*.

I. INTRODUCTION

Titanium dioxide, TiO_2, nanoparticles (NPs) involving a mixture of anatase and rutile polymorphs, in particular, in the commercialized Degussa P25 form, constitute the most studied photocatalytic material and a model system for the mechanisms involved in photocatalysis.[1–4] The performance of TiO_2 depends largely on its optical, electronic, structural, morphological, and surface properties,[5–7] and one of the key properties of TiO_2, especially in the anatase polymorph, is the formation of photogenerated charge carriers (holes and electrons) activated by the absorption of ultraviolet (UV) light. Indeed, the need for UV radiation constitutes one of the major bottlenecks toward developing efficient TiO_2 photocatalysts that can work under sunlight, as only ~5% of the incident solar spectrum corresponds to UV light. Hence, a major challenge in the development of competitive TiO_2-based photocatalysts is reducing the energy gap to the visible (VIS) region.[8]

In principle, the properties of TiO_2 can be modulated by designing NPs with different sizes, shapes, crystallinities, and surface facets.[9–12] However, to determine the relationship between structural and electronic properties of TiO_2 nanoparticles, experimentally, is not a simple task. Alternatively, computational techniques provide a feasible, accurate, and unbiased approach to study such correlations and, consequently, can contribute to building connections between experiment and theory.[13]

Density functional theory (DFT)[14,15] has been widely used to study the properties of different types of materials with high accuracy in the prediction of crystal structures and reasonable

description of electronic structure features at a moderate computational cost[16] and with a well-established reproducibility.[17] Unfortunately, energy gaps computed using the popular local density approximation (LDA) and the generalized gradient approximation (GGA) are consistently underestimated by 30%–100%.[18,19] The error arises from the inherent lack of derivative discontinuity and the delocalization error.[20–22] To overcome the drawbacks of LDA and GGA for estimating this electronic property, hybrid functionals, which include a part of the nonlocal Fock exchange, have been proposed and widely employed.[18,23,24] Depending on the type of basis set, the use of hybrid functionals can represent a significant increase in the cost of the calculations. Inspired by the Hubbard Hamiltonian,[25] Anisimov *et al.*[26] proposed to avoid the computational load inherent to hybrid functionals by implementing an empirical on-site Hubbard (U) correction to a selected atomic energy level, within standard DFT. The resulting method is often referred to as DFT+U, an unfortunate term as DFT is an exact theory. DFT+U has been broadly used, especially after the contribution of Dudarev *et al.*[27] and is particularly useful in the description of the partially filled d-states of the transition metals—in the case of TiO_2, the U-correction is applied to the Ti 3d orbital.[28,29]

The DFT+U method combines the high efficiency of standard DFT with an explicit, albeit approximate and empirical, treatment of electron on-site correlation and constitutes one of the simplest approaches to describe the ground state of strongly correlated systems.[30] However, the choice of appropriate U parameter value for each compound is a challenge. This obstacle can be solved through (i) a linear response, fully consistent method[31] or (ii) alternative routes based on comparison with experimental results for some physical property of interest, such as magnetic moment, energy gap, redox potentials, or reaction enthalpies.[32–34] For instance, the latter strategy has been employed in the study of the electron transport in the rutile phase,[35,36] reduced forms of TiO_2,[37,38] and ultrathin films of the rutile phase.[39] Nevertheless, the selection of the U parameter is not straightforward. Moreover, the choice of the appropriate form of the projector functions inherent to the method is also a concern,[40] especially after the work of Kick *et al.*[41] who recently implemented DFT+U with a numerical atomic orbital (NAO) basis set. The authors showed that the value for U depends on the choice of projector function, which, in turn, depends on the type of basis set [atomic orbitals or plane waves (PWs)] used. The aim of the current study is to evaluate the effect of the basis sets in the selection of the U value necessary to describe the electronic structure of semiconducting nanoparticles, taking a previously investigated, well-defined $(TiO_2)_{35}$ bipyramidal NP as a case study.[42]

Nanoparticles exhibit features that are not present in bulk or extended surface models; these include large surface areas, low-coordinated surface sites, and quantum confinement effects. Such features endow NPs with unique properties, which make them of interest, in particular, for photocatalytic applications.[43] TiO_2 NPs have been the subject of a number of DFT studies at different levels of the theory.[44–52] An understanding of the performance of different implementations of DFT in the description of the structural and electronic properties of isolated nanoparticle systems is crucial for the effective application of computational methods.

II. MODELS AND COMPUTATIONAL METHODS

The well-defined bipyramidal stoichiometric $(TiO_2)_{35}$ anatase NP, which fulfills the requirement of a Wulff construction,[53] and was used in previous studies,[42] is selected for the present study (Fig. 1). This nanoparticle exposes the most favorable (101) facets only, as found in experiments.[7] Furthermore, its ~2 nm size is also appropriate to rationalize the experimental results reported for TiO_2 anatase NPs.[54]

The calculations reported here have been carried out using two widely used codes, namely, the Vienna *Ab Initio* Simulation Package (VASP)[55,56] and the Fritz Haber Institute *ab initio* molecular simulations (FHI-aims).[57] In both cases, the Perdew–Wang (PW91) exchange–correlation functional[58] is used, and spin-polarization is accounted for explicitly, although the final results do not exhibit any spin-polarization. The partially filled Ti_{3d} states were consistently described by applying the Hubbard U correction[26] under the simplified rotationally invariant approach introduced by Dudarev *et al.*[27] In the following, we will refer to the resulting approach as PW91+U, which is more appropriate. The calculations carried out with VASP employ a plane waves (PWs) basis set with a kinetic energy cutoff of 396 eV. To account for the effect of inner electrons on the valence density, we implement the projector augmented wave (PAW) method of Blöch,[59] as implemented by Kresse and Joubert,[60]

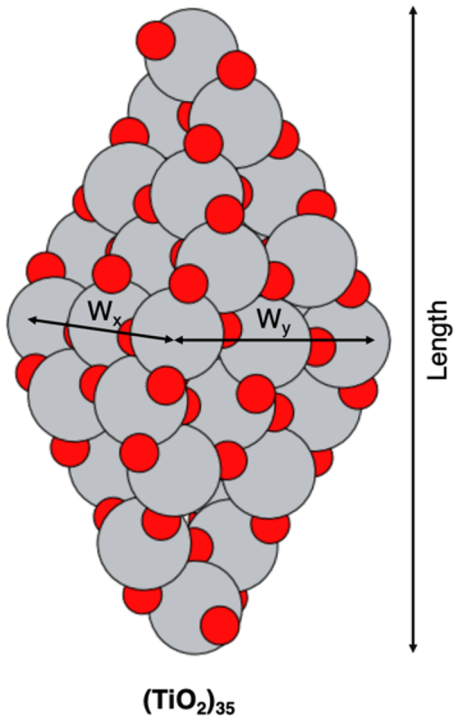

FIG. 1. Stoichiometric $(TiO_2)_{35}$ anatase NP with bipyramidal morphology. All the exposed facets correspond to the (101) surface. The dimensions of the NP are indicated with double arrows. W_x and W_y denote the nanoparticle width in the x and y directions, respectively. Gray and red spheres represent Ti and O atoms, respectively.

with 12 and 6 valence electrons for Ti and O atoms, respectively. The $(TiO_2)_{35}$ NP is included in a 20 × 20 × 40 Å supercell to give a vacuum gap of 11 Å in the *x*- and *y*-directions and 20 Å in the *z*-direction. Γ-point sampling is used, and the convergence criteria for the energy and forces are 10^{-4} eV/Å^{-2} and 0.02 eV/Å^{-2}, respectively.

On the other hand, the calculations carried out by the FHI-aims code include all electrons (AEs) and account for relativistic effects through the so-called zero-order regular approximation (ZORA)[61,62] proposed earlier by Chang *et al.*[63] A tier-1 light grid numerical atom-centered orbital (NAO) basis set has been used, with a quality comparable to that of a TZVP Gaussian type orbital basis set for TiO_2.[42] Here, for the implementation of Hubbard *U* correction, the projection functions for Ti_{3d} states are introduced as an explicit linear combination of the NAO basis functions with the double-counting correction in the fully localized limit (FLL) (see details in Ref. 41). The convergence threshold for the energy is 10^{-4} eV. Note that, hereinafter, the notation of PW and NAO is used to refer to the calculations performed with VASP and FHI-aims, respectively.

III. RESULTS AND DISCUSSION

To provide a sound reference for the study, we first discuss the energy gap of fully relaxed anatase and rutile bulk phases as predicted from spin polarized DFT calculations with the PW91 GGA type density functional and using either PW or NAO basis sets. To avoid problems arising from a difference in the quality of the basis sets, we increase the kinetic energy cutoff for the PW to 550 eV and used a more extended NAO basis set of tier-2 tight quality. For rutile, the PW/NAO calculated bandgap is 1.94/1.91 eV, whereas for anatase, the PW/NAO calculated bandgap amounts to 2.25/2.10 eV. The difference in the anatase phase must be attributed to small differences in the optimized structure arising from the different treatment of the core electrons. In any case, the PW and NAO calculations for bulk rutile and anatase lead essentially to the same results with a deviation of at most 0.15 eV in the bandgap. Clearly, these calculated energy gaps are underestimated with respect to the experimental values, which are 3.0 eV and 3.2 eV for rutile and anatase phases, respectively.[64–66] Hybrid functionals with an *ad hoc* amount of non-local Fock exchange are known to provide a better estimate, as discussed for instance by Ko *et al.*[67] In this paper, based on calculations performed with FHI-aims, the authors tuned the percentage of Fock exchange in the PBE0 hybrid functional to reproduce the experimental bandgap of bulk rutile and anatase TiO_2. With 12.5% of Fock exchange, denoted as PBEx, the bandgap of anatase was computed as 3.22 eV. A similar computational setup in VASP yields a value of 3.21 eV for the bulk anatase energy gap. While DFT+*U* can also be tuned to recover the experimental bandgap, this is usually at the cost of a poorer description of other materials properties.

Next, we focus on the representative $(TiO_2)_{35}$ anatase NP depicted in Fig. 1. The atomic structure of this NP has been obtained from a geometry optimization using both VASP and FHI-aims computational packages and PW91+*U*. However, to perform a rigorous comparison of the effect of *U* when using PW or NAO basis sets, we consider four different situations, which are as follows:

(i) The structure is optimized in FHI-aims with PW91 ($U = 0$), and single-point calculations are run with both FHI-aims and VASP at each *U* value, $U = 0$–10 eV.
(ii) The structure is optimized in VASP with PW91 ($U = 0$), and single-point calculations are run with both FHI-aims and VASP at each *U* value, $U = 0$–10 eV.
(iii) The structure is fully optimized in both FHI-aims and VASP at each $U = 0$–10 eV.
(iv) Each structure obtained by FHI-aims (VASP) in (iii) is submitted to a single point calculation in VASP (FHI-aims) at the same *U*-value.

The first and second sets of calculations allow one to investigate differences in the description of the electronic structure, which are not due to a difference in the atomic structure, but to the different type of basis set and the implementation of the +*U* term.[41] The third set of calculations provides information about differences in the final optimized structure, and the effect of this optimization on the energy gap. Finally, the fourth set of calculations shows that to what extent the fully relaxed atomic structure impacts on the electronic structure. In each of these datasets, we can compare the results of the different setups by a linear fit of the data.

A. Structure analysis

We start the discussion by analyzing the structural properties of the $(TiO_2)_{35}$ NPs focusing mainly on its length and width (Fig. 2). The PW91 ($U = 0$) fully optimized structures of the $(TiO_2)_{35}$ NPs predicted by VASP and FHI-aims are almost the same. In both cases, the nanoparticle length, which is taken from the terminal atoms located in the apical region (see Fig. 1), is 19.61 Å. For the width of the NPs, FHI-aims predicts a width that is 0.02 Å larger than VASP. Hence, in the absence of *U*, both types of basis sets lead to the same structure, as expected.[17]

Therefore, any difference in the PW91+*U* structure predicted by the two types of basis sets (codes) has to be attributed to differences in the implementation of *U*. Regarding the atomic structure, the main effect of *U* is to slightly increase the nanoparticle length [Fig. 2(a)]. The tendency is consistent, regardless of the basis set, up to $U = 5$ eV. When *U* is larger than 5 eV, the lengths predicted by VASP and FHI-aims follow different trends. The analysis of the nanoparticle width presents some interesting features [Figs. 2(b) and 2(c)]. Here, the effect of *U* is different depending on whether the calculation is carried out with a PW or NAO basis set. When using NAO, the optimized NP width decreases almost linearly with increasing *U* up to $U = 7$ eV, whereas when using PW, the dependence with *U* is very small, almost negligible. We note that, when using PW, the trends are very stable along the interval of *U*. However, this is not the case when the NAO basis set is employed, and the regular trend is broken at $U = 7$ eV. Note also that the breaking of the trend at $U > 7$ eV for the NAO calculations indicates that this value is too large to correctly describe correlation effects, as it has an exceedingly large influence on the properties of the nanoparticle and induces structural discontinuities. Similar observations on the effect of *U* on the phase stability of TiO_2 have been reported.[33] It is assumed that the large effect of *U* on the atomic structure predicted by the calculations using the NAO basis set arises from the

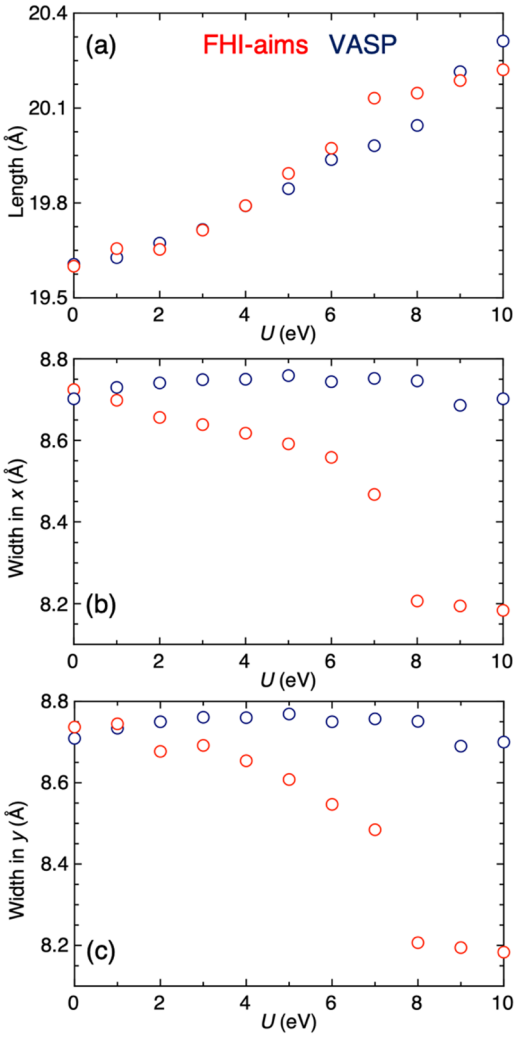

FIG. 2. Evolution of the dimensionality of the stoichiometric $(TiO_2)_{35}$ anatase NP based on (a) length, (b) width in *x*, and (c) width in *y* as a function of the *U* parameter for fully optimized structures by using VASP (blue dots) and FHI-aims (red dots) codes.

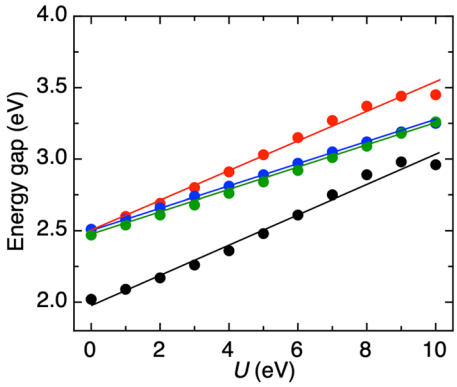

FIG. 3. Variation of the energy gap with the parameter of *U*. The energy gap trends of [scenario (i)] optimized $(TiO_2)_{35}$ anatase NP with the FHI-aims code at $U = 0$ eV are calculated by performing single point calculations with the FHI-aims code (red) and VASP (green) and [scenario (ii)] optimized structure with the VASP code at $U = 0$ eV by using single point calculations with FHI-aims (black) and VASP (blue). Details of the linear fit ($E_{gap} = aU + b$) data for each trendline are listed in Table I.

more localized character of the atomic NAO Hubbard projectors, as implemented in FHI-aims.[41]

B. Energy gap analysis

The analysis of the energy gap of the $(TiO_2)_{35}$ anatase NPs provides further interesting comparisons. The Kohn–Sham energy gaps, computed in the setups described in scenarios (i) and (ii), are shown in Fig. 3 and Table I. These data correspond to two structures, each optimized with the respective codes, FHI-aims and VASP, at the PW91 ($U = 0$) level. We begin by comparing the results of the single-point PW calculations performed on the FHI-aims (green) and VASP (blue) relaxed structures. At each *U*-value, the difference in computed energy gap between the two structures is negligible; in this case, the PW basis set implementation of $+U$ is not sensitive to the geometry at which the electronic structure is computed.

This result contrasts with the NAO data: for each *U*-value, NAO calculations predict a larger energy gap for the FHI-aims structure, relative to the VASP structure. The energy gaps computed from single point NAO calculations over the FHI-aims relaxed structure (red) are positively offset by ~0.5 eV with respect to those values computed over the VASP relaxed structure (black). The change in the energy gap with increasing *U* is consistent, regardless of the atomic structure, as revealed by the slopes (*a*-values) of the red and black trendlines, presented in Table I, i.e., the 0.5 eV offset is maintained over the range of *U*-values. This result is interesting because, as discussed, both FHI-aims and VASP predict similar structures, viz., length and width, at the PW91 ($U = 0$) level. However, small differences in the atomic structures yield appreciable differences in the energy gaps computed with the NAO basis set, while no differences were shown with the PW basis set. This highlights that to avoid misunderstanding interpretations in the analysis of the electronic properties, structural relaxation is crucial when using the NAO basis set. It appears that the impact of *U* is greater with NAO, related to the localized projector functions.[41]

It is also interesting to compare NAO and PW results when these calculations are performed on the same starting structure. For the FHI-aims relaxed structure, the energy gaps predicted by NAO (red) and PW (green) calculations are in agreement for small *U*-values, but the differences in the predicted gaps increase with increasing *U*. This is reflected in the slopes (*a*-values) of the trendlines fitted to the NAO (red) and PW (green) data, which are 0.103 and 0.075, respectively (see Table I). In this case, the energy gap varies to a greater extent in the NAO calculations, which consistently predict larger gaps with respect to the PW calculations. Conversely, for the VASP relaxed structure, the energy gaps predicted by NAO (black) and PW (blue) differ over the entire range of considered *U*-values. For $U = 0$ eV, the PW-computed energy gap is larger than that computed with NAO by ~0.5 eV, but this difference decreases

TABLE I. Linear fit ($E_{gap} = aU + b$) data for (i) optimized $(TiO_2)_{35}$ anatase NPs with the FHI-aims code at $U = 0$ eV are calculated by performing single point calculations with the FHI-aims code (red) and VASP (green) and (ii) the optimized structure with the VASP code at $U = 0$ eV by using single point calculations with FHI-aims (black) and VASP (blue) shown in Fig. 3.

	Plot legend		Trendline		
	Structure	Single-point	a	b (eV)	R^2
Red	FHI-aims ($U = 0$)	FHI-aims (each U)	0.103	2.510	0.989
Green	FHI-aims ($U = 0$)	VASP (each U)	0.075	2.510	0.999
Black	VASP ($U = 0$)	FHI-aims (each U)	0.106	1.980	0.984
Blue	VASP ($U = 0$)	VASP (each U)	0.080	2.450	0.998

with increasing U, in accordance with the larger slope for the NAO data (0.106), with respect to that of the PW data (0.080). These results suggest that the differences observed in the computed Kohn–Sham energy gaps are not attributable to differences in the atomic structure, but rather to differences in the implementation of DFT+U for the NAO or PW basis set.

Finally, we note that each of the computational setups, with the exception of NAO calculations on the VASP relaxed structure (black), predicts similar energy gaps of ~2.5 eV for $U = 0$ eV. For these three setups, the differences in the computed energy gaps are reasonable, i.e., within 0.15 eV, for U-values up to 4 eV. For $U > 4$ eV, the NAO basis set promotes a larger energy gap with respect to the PW basis set.

The data obtained from the calculations described in scenarios (iii) and (iv) are presented in Fig. 4 and Table II. We first look at the computed energy gaps for the structures optimized at each U-value in FHI-aims (red) and VASP (blue). The energy gaps computed with the NAO basis set increase from 2.5 eV to 3.8 eV as U increases from 0 eV to 10 eV. This monotonic increase with U is expected and is corroborated in the trendline data, shown in Table II.

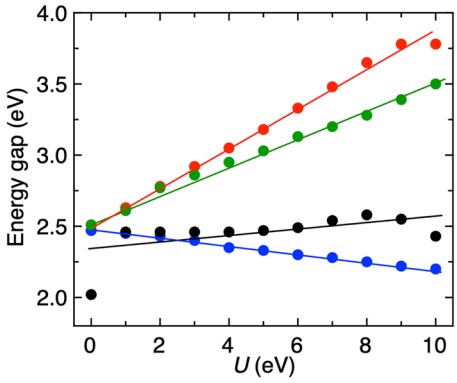

FIG. 4. Variation of the energy gap with the parameter of U for [scenario (iii)] the fully optimized $(TiO_2)_{35}$ anatase NPs with the FHI-aims code (red) and VASP code (blue) and [scenario (iv)] single-point calculations in VASP (green) on the FHI-aims relaxed structure for each U and single-point calculations in FHI-aims (black) on the VASP-relaxed structure at each U. Details of the linear fit ($E_{gap} = aU + b$) data for each trend-line are listed in Table II.

Interestingly, the opposite trend is observed for the energy gaps computed for the structures that were fully relaxed at each U with the PW basis set: in this case, the energy gaps decrease monotonically with increasing U. As seen in our discussion of Fig. 3, increasing the U-value in a PW calculation on a fixed structure yields a larger energy gap. Thus, here, we must attribute the decrease in the energy gaps to effects arising from the structural optimization at each U. This result is surprising, not only because it is unexpected, but also because the changes in the PW-computed atomic structures over the range of U-values are modest (see Fig. 2), yet the impact on the electronic structure is significant, with states in the gap attributed to the presence of the low coordinated O atoms (see Fig. 5). In fact, for the VASP-relaxed PW91 ($U = 0$) structure, a single-point PW calculation with $U = 4$ eV yields an energy gap of 2.76 eV, whereas for the fully relaxed structure at $U = 4$ eV, the energy gap is 2.35 eV. In other words, the emergence of the gap states occurs at lower U values in the PW calculations. This is clearly seen in the results in Fig. 5 corresponding to the VASP and FHI-aims calculations for $U = 2$ eV and 6 eV, respectively.

Performing a single-point PW calculation on the FHI-aims relaxed structures at each U-value produces the energy gaps represented with the green data points in Fig. 4. Here, we see that the data points agree with those computed with the NAO basis set (red) within 0.1 eV up to $U = 4$ eV after which the differences increase. This is in agreement with the trendline data listed in Table II; the slopes for the NAO (red) and PW (green) basis sets are 0.136 and 0.095, respectively. Importantly, single-point PW calculations on the FHI-aims relaxed structures, at each U, predict an increase in energy gap with increasing U. This further confirms that the decreasing trend in energy gaps for the VASP-relaxed structures arises from structural effects.

The energy gaps computed with single-point NAO calculations on the VASP-relaxed structures, at each U, are shown with the black data points in Fig. 4. An outlier in these data is the energy gap computed for $U = 0$ eV, which is 2.02 eV. This value has been checked, and the presence of an error in the calculation can be ruled out. Note, in addition, that the main effect of this calculation comes from the structural relaxation performed with VASP. Interestingly, for $U = 1$–10 eV, the computed energy gaps are consistently ~2.5–2.6 eV, and these data show no discernible increasing or decreasing trend. Unlike the case of $U = 0$ eV, the structural effect induced by a previous relaxation with VASP is coupled to the U implementation as

TABLE II. Linear fit ($E_{gap} = aU + b$) data for (iii) the fully optimized $(TiO_2)_{35}$ anatase NPs with the FHI-aims code (red) and VASP code (blue) and (iv) single-point calculations in VASP (green) on the FHI-aims relaxed structure for each U and single-point calculations in FHI-aims (black) on the VASP-relaxed structure at each U shown in Fig. 4.

	Plot legend		Trendline		
	Structure	Single-point	a	b (eV)	R^2
Red	FHI-aims (each U)	...	0.136	2.520	0.993
Green	FHI-aims (each U)	VASP (each U)	0.095	2.550	0.994
Black	VASP (each U)	FHI-aims (each U)	0.027	2.310	0.358
Blue	VASP (each U)	...	−0.028	2.450	0.994

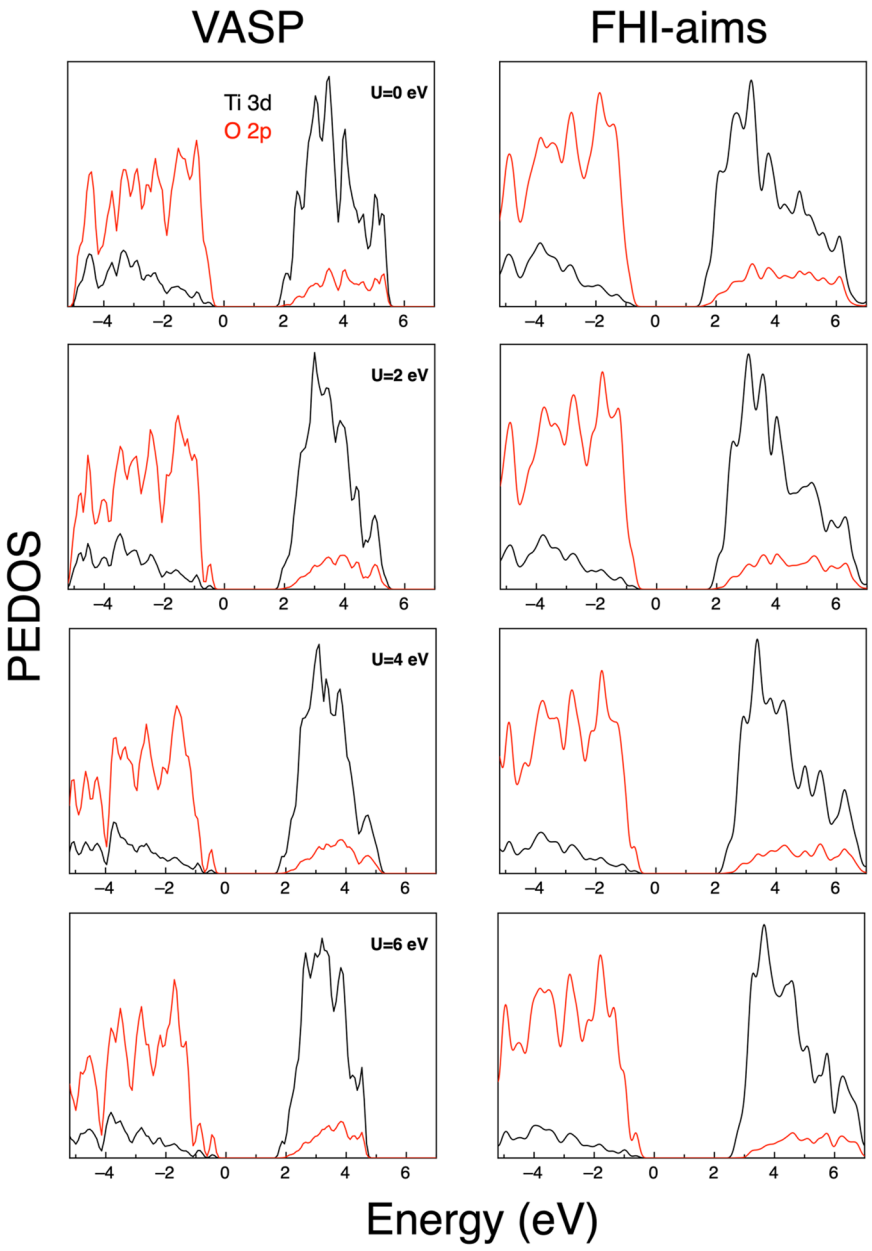

FIG. 5. Projected electronic density of states (PEDOS) of the full relaxed $(TiO_2)_{35}$ NPs using PW and NAO basis sets for U = 0 eV, 2 eV, 4 eV, and 6 eV.

implemented in FHI-aims. As seen in our discussion of single-point NAO calculations on both the FHI-aims and VASP PW91 ($U = 0$) relaxed structures, the predicted energy gaps increase monotonically with increasing U. Once again, this suggests that subtleties in the structural optimization within the PW implementation of DFT+U, probably linked to the low coordinated O atoms at the NP edge, produce these effects in the electronic structure.

For the NAO calculations, consistent with the linear trends for the red data reported in the legends of Figs. 3 and 4, the relaxation at each U value has a negligible effect, as expected, on the fitting offset with respect to the calculation at the PW91 ($U = 0$) structure. However, the fully relaxed calculations result in changes in the fitting slope. Thus, the opening of the energy gap is more pronounced for the fully optimized structures when employing the NAO basis.

This latter situation, where the NP structure is fully relaxed at each U in each code, is the most reasonable scenario to analyze the different behaviors observed between basis sets because artifacts due to the use of a structure not optimized within the method/basis set are ruled out. First of all, the energy gaps between the PW and NAO basis set are shifted by 0.25 eV (see Fig. 3), which can be attributed to a different treatment of the effect of the core electrons and also relativistic effects.[68,69] The former are included explicitly in the calculations with the NAO basis set, whereas they are included through a frozen orbital type approach through the PAW in the calculations with the PW basis. Similarly, the relativistic effects are included explicitly at the ZORA level with the NAO basis and implicitly through the PAW description of the core electrons in the PW calculations. In principle, the most accurate results are obtained from the all-electron basis set implemented in FHI-aims. The most relevant results are found in the variation of the energy gap in response to increasing U. These are depicted in Fig. 4, and the trends (Table II) are reflected in the linear fittings, with slopes of 0.136 and −0.028 for NAO and PW basis set, respectively. This result clearly shows that the effect of U on the resulting energy gap does not only depend on the numerical value of this parameter but also on the projection of the Kohn–Sham states to determine the occupation numbers that enter the $+U$ correction and the structural optimization, which, in turn, depend on the basis set used. Thus, the $+U$ part of the exchange–correlation potential severely depends on the DFT code, as already shown by Kick *et al.* for some systems.[41]

To clarify this issue, we comment on how results from the PW91+U approaches used in the present work can compare to those corresponding to synthetized bipyramidal TiO_2 NPs containing almost 90% of (101) facets that morphologically match quite well with the $(TiO_2)_{35}$ NP model depicted in Fig. 1. UV–Vis diffuse reflectance spectroscopy reported an energy gap of ~3.2 eV.[70] To reproduce this result using PW91+U requires a U value between 4 eV and 5 eV for the NAO basis set. No U-value can reproduce this energy gap for the optimized structures with a PW basis set; however, U = 8–9 eV, implemented with a single-point PW calculation on the PW91 ($U = 0$) structure does reproduce the experiments. Therefore, the DFT+U implementation in FHI-aims entails much lower values of U to reproduce results obtained with other codes such as VASP. This is attributed to the strongly localized character of the atomic NAO Hubbard projectors. In short, to achieve a given bandgap, the value of U that is required is much lower with the NAO basis set compared to the PW basis set. In addition, we compare the experiments[70] with the hybrid PBEx (12.5% Fock exchange) density functional on the $(TiO_2)_{35}$ NPs. FHI-aims and VASP yields energy gaps of 3.81[46] and 3.71 eV, respectively. Not surprisingly, these values exceed the experimental evidences due to the quantum confinement effect.[12]

Finally, to confirm that the present findings are not specific to the $(TiO_2)_{35}$ nanoparticle, we consider the anatase bulk phase and explore the transferability of U for calculations with PAW or NAO basis for a particular geometry. Hence, structural optimizations of the anatase bulk phase were first performed by using PW basis set and an energy gap of 3.17 eV, close to the experimental value, was achieved for $U = 8$ eV. Next, this structure was considered in NAO single point calculations to determine the U value that reproduces the energy gap and this was $U = 6.5$ eV. This confirms that the U value fitted to reproduce an experimental or hybrid functional calculated value using a given DFT code cannot be transferred to another code as it depends on the basis set used and on the method employed to define the corresponding projectors. Thus, for each materials system and DFT code, one should recompute suitable values for U through making initial benchmarks.

IV. CONCLUSIONS

The effect of the DFT+U method on the structural and electronic properties of the $(TiO_2)_{35}$ NPs is systematically investigated by two different basis sets, namely, plane-waves (PWs) and numerical atomic orbitals (NAOs), along with different approaches for the implementation of the $+U$ value. In the absence of U, PW and NAO calculations report the same structure, and consequently, the structural variations observed by its inclusion are due to the different implementation of U based on a simplified rotationally invariant approach and a linear combination of the NAO basis functions, respectively. Interestingly, the analysis of the energy gap reveals that a certain U value can reproduce the experimental value; however, it depends on the basis set and on the employed U parameter. Therefore, the transfer of U values between codes is not to be recommended and requires initial benchmarks for the property of interest as a reference to find the appropriate value. This study clearly shows that the DFT+U implementation in a localized basis set code such as FHI-aims entails much lower values of U to reproduce the results obtained with a plane wave basis set code such as VASP.

AUTHORS' CONTRIBUTIONS

Á.M.-G. and S.R. contributed equally to this work.

ACKNOWLEDGMENTS

We thank Matthias Kick for the technical discussion during the elaboration of FHI-aims calculations. The research reported in this work was supported by the Spanish No. MICIUN RTI2018-095460-B-I00 and *María de Maeztu* No. MDM-2017-0767 grants and, in part, by Generalitat de Catalunya No. 2017SGR13. Á.M.-G. thanks Spanish MICIUN for a *Juan de la Cierva* postdoctoral Grant (No. IJCI-2017-31979) and F.I. acknowledges additional support

from the 2015 ICREA Academia Award for Excellence in University Research. S.R. and M.N. acknowledge support from the Science Foundation Ireland through the ERA.Net for Materials Research and Innovation (M-ERA.Net 2), Horizon 2020 Grant Agreement No. 685451, and SFI Grant No. SFI/16/M-ERA/3418 (RATOCAT). We acknowledge access to SFI funded computing resources at the Tyndall Institute and the SFI/HEA funded Irish Centre for High End Computing (ICHEC). We also acknowledge COST Action No. CA18234.

The authors have no conflicts of interest to declare.

DATA AVAILABILITY

The data that support the findings of this study are available from the corresponding author upon reasonable request.

REFERENCES

[1] T. Ohno, K. Sarukawa, K. Tokieda, and M. Matsumura, J. Catal. **203**, 82 (2001).
[2] A. Fujishima, T. N. Rao, and D. A. Tryk, J. Photochem. Photobiol., C **1**, 21 (2000).
[3] A. Fujishima, T. N. Rao, and D. A. Tryk, Electrochim. Acta **45**, 4683 (2000).
[4] K. Hashimoto, H. Irie, and A. Fujishima, Jpn. J. Appl. Phys., Part 1 **44**, 8269 (2005).
[5] M. Gao, L. Zhu, W. L. Ong, J. Wang, and G. W. Ho, Catal. Sci. Technol. **5**, 4703 (2015).
[6] A. Naldoni, M. Altomare, G. Zoppellaro, N. Liu, Š. Kment, R. Zbořil, and P. Schmuki, ACS Catal. **9**, 345 (2019).
[7] D. Cho, K. C. Ko, O. Lamiel-García, S. T. Bromley, J. Y. Lee, and F. Illas, J. Chem. Theory Comput. **12**, 3751 (2016).
[8] X. Chen, L. Liu, P. Y. Yu, and S. S. Mao, Science **331**, 746 (2011).
[9] X. Chen and S. S. Mao, Chem. Rev. **107**, 2891 (2007).
[10] X. Chen, C. Li, M. Grätzel, R. Kostecki, and S. S. Mao, Chem. Soc. Rev. **41**, 7909 (2012).
[11] D. Selli, G. Fazio, and C. Di Valentin, Catalysts **7**, 357 (2017).
[12] Á. Morales-García, A. Macià Escatllar, F. Illas, and S. T. Bromley, Nanoscale **11**, 9032 (2019).
[13] E. Clot, Dalton Trans. **43**, 11092 (2014).
[14] W. Kohn and L. J. Sham, Phys. Rev. **140**, A1133 (1965).
[15] P. Hohenberg and W. Kohn, Phys. Rev. **136**, B864 (1964).
[16] K. Burke, J. Chem. Phys. **136**, 150901 (2012).
[17] K. Lejaeghere, G. Bihlmayer, T. Björkman, P. Blaha, S. Blügel, V. Blum, D. Caliste, I. E. Castelli, S. J. Clark, A. Dal Corso *et al.*, Science **351**, aad3000 (2016).
[18] I. de P. R. Moreira, F. Illas, and R. L. Martin, Phys. Rev. B **65**, 155102 (2002).
[19] C. S. Wang and W. E. Pickett, Phys. Rev. Lett. **51**, 597 (1983).
[20] L. J. Sham and M. Schlüter, Phys. Rev. Lett. **51**, 1888 (1983).
[21] P. Mori-Sánchez and A. J. Cohen, Phys. Chem. Chem. Phys. **16**, 14378 (2014).
[22] P. Mori-Sánchez, A. J. Cohen, and W. Yang, Phys. Rev. Lett. **100**, 146401 (2008).
[23] J. Muscat, A. Wander, and N. M. Harrison, Chem. Phys. Lett. **342**, 397 (2001).
[24] A. D. Becke, J. Chem. Phys. **98**, 1372 (1993).
[25] J. Hubbard, Proc. R. Soc. London, Ser. A **276**, 238 (1963).
[26] V. I. Anisimov, J. Zaanen, and O. K. Andersen, Phys. Rev. B **44**, 943 (1991).
[27] S. L. Dudarev, G. A. Botton, S. Y. Savrasov, C. J. Humphreys, and A. P. Sutton, Phys. Rev. B **57**, 1505 (1998).
[28] N. S. Portillo-Vélez, O. Olvera-Neria, I. Hernández-Pérez, and A. Rubio-Ponce, Surf. Sci. **616**, 115 (2013).
[29] M. T. Curnan and J. R. Kitchin, J. Phys. Chem. C **119**, 21060 (2015).
[30] L. Wang, T. Maxich, and G. Ceder, Phys. Rev. B **73**, 195107 (2006).
[31] M. Cococcioni and S. de Gironcoli, Phys. Rev. B **71**, 035105 (2005).
[32] C. Loschen, J. Carrasco, K. M. Neyman, and F. Illas, Phys. Rev. B **75**, 035115 (2007).
[33] M. E. Arroyo-de Dompablo, A. Morales-García, and M. Taravillo, J. Chem. Phys. **135**, 054503 (2011).
[34] Z. Hu and H. Metiu, J. Phys. Chem. C **115**, 5841 (2011).
[35] N. A. Deskins and M. Dupuis, Phys. Rev. B **75**, 195212 (2007).
[36] C. Persson and A. Ferreira da Silva, Appl. Phys. Lett. **86**, 231912 (2005).
[37] E. Finazzi, C. Di Valentin, G. Pacchioni, and A. Selloni, J. Chem. Phys. **129**, 154113 (2008).
[38] B. J. Morgan and G. W. Watson, J. Phys. Chem. C **114**, 2321 (2010).
[39] G. Barcaro, I. O. Thomas, and A. Fortunelli, J. Chem. Phys. **132**, 124703 (2010).
[40] B. Himmetoglu, A. Floris, S. de Gironcoli, and M. Cococcioni, Int. J. Quantum Chem. **114**, 14 (2014).
[41] M. Kick, K. Reuter, and H. Oberhofer, J. Chem. Theory Comput. **15**, 170 (2019).
[42] O. Lamiel-García, K. C. Ko, J. Y. Lee, S. T. Bromley, and F. Illas, J. Chem. Theory Comput. **13**, 1785 (2017).
[43] Y. Nam, J. H. Lim, K. C. Ko, and J. Y. Lee, J. Mater. Chem. A **7**, 13833 (2019).
[44] F. Nunzi, S. Agrawal, A. Selloni, and F. De Angelis, J. Chem. Theory Comput. **11**, 635 (2015).
[45] Á. Morales-García, R. Valero, and F. Illas, Phys. Chem. Chem. Phys. **20**, 18907 (2018).
[46] S. Kim, K. C. Ko, J. Y. Lee, and F. Illas, Phys. Chem. Chem. Phys. **18**, 23755 (2016).
[47] Z.-W. Qu and G.-J. Kroes, J. Phys. Chem. B **110**, 8998 (2006).
[48] M.-H. Weng, C. Chen, and S.-P. Ju, Chin. J. Catal. **30**, 384 (2009).
[49] K. Morita and K. Yasuoka, AIP Adv. **8**, 035119 (2018).
[50] Á. Morales-García, R. Valero, and F. Illas, J. Chem. Theory Comput. **13**, 3746 (2017).
[51] R. Valero, Á. Morales-García, and F. Illas, J. Chem. Theory Comput. **14**, 4391 (2018).
[52] Á. Morales-García, R. Valero, and F. Illas, J. Chem. Theory Comput. **15**, 5024 (2019).
[53] G. Wulff, Z. Kristallogr. - Cryst. Mater. **34**, 44 (1901).
[54] S. Pigeot-Rémy, F. Dufour, A. Herissan, V. Ruaux, F. Maugé, R. Hazime, C. Foronato, C. Guillard, C. Chaneac, O. Durupthy, C. Colbeau-Justin, and S. Cassaignon, Appl. Catal., B **203**, 324 (2017).
[55] G. Kresse and J. Hafner, Phys. Rev. B **49**, 14251 (1994).
[56] J. Furthmüller, J. Hafner, and G. Kresse, Phys. Rev. B **53**, 7334 (1996).
[57] V. Blum, R. Gehrke, F. Hanke, P. Havu, V. Havu, X. Ren, K. Reuter, and M. Scheffler, Comput. Phys. Commun. **180**, 2175 (2009).
[58] J. P. Perdew, K. Burke, and Y. Wang, Phys. Rev. B **54**, 16533 (1996).
[59] P. E. Blöchl, Phys. Rev. B **50**, 17953 (1994).
[60] G. Kresse and D. Joubert, Phys. Rev. B **59**, 1758 (1999).
[61] E. van Lenthe, R. van Leeuwen, E. J. Baerends, and J. G. Snijders, Int. J. Quantum Chem. **57**, 281 (1994).
[62] M. K. Y. Chan and G. Ceder, Phys. Rev. Lett. **105**, 196403 (2010).
[63] C. Chang, M. Pelissier, and P. Durand, Phys. Scr. **34**, 394 (1986).
[64] A. Amtout and R. Leonelli, Phys. Rev. B **51**, 6842 (1995).
[65] S. P. Kowalczyk, F. R. McFeely, L. Ley, V. T. Gritsyna, and D. A. Shirley, Solid State Commun. **23**, 161 (1977).
[66] D. O. Scanlon, C. W. Dunnill, J. Buckeridge, S. A. Shevlin, A. J. Logsdail, S. M. Woodley, C. R. A. Catlow, M. J. Powell, R. G. Palgrave, I. P. Parkin, G. W. Watson, T. W. Keal, P. Sherwood, A. Walsh, and A. A. Sokol, Nat. Mater. **12**, 798 (2013).
[67] K. C. Ko, O. Lamiel-García, J. Y. Lee, and F. Illas, Phys. Chem. Chem. Phys. **18**, 12357 (2016).
[68] G. B. Bachelet and N. E. Christensen, Phys. Rev. B **31**, 879 (1985).
[69] B. Sadigh, A. Kutepov, A. Landa, and P. Söderlind, Appl. Sci. **9**, 5020 (2019).
[70] M. D'Arienzo, M. V. Dozzi, M. Redaelli, B. Di Credico, F. Morazzoni, R. Scotti, and S. Polizzi, J. Phys. Chem. C **119**, 12385 (2015).